

Vibration of a Singly-Curved Thin Shell Reflector with a Unidirectional Tension Field

R. Brett Williams,^{*} Kerry J. Klein[†], and Gregory S. Agnes[‡]

* Member of Technical Staff, Jet Propulsion Laboratory, 4800 Oak Grove Dr., MS 299-101, Pasadena, CA 91109: rowilli6@jpl.nasa.gov

† Associate Member of Technical Staff, Jet Propulsion Laboratory: kerry.j.klein@jpl.nasa.gov

‡ Senior Member of Technical Staff, Jet Propulsion Laboratory: gregory.s.agnes@jpl.nasa.gov

Abstract

Increased science requirements for space-based instruments over the past few decades have lead to the increased popularity of deployable space structures constructed from thin, lightweight films. Such structures offer both low mass and the ability to be stowed inside conventional launch vehicles. The analysis in this work pertains to large, singly-curved lightweight deployable reflectors commonly used in radar antennas and space telescopes. These types of systems, which can vary a great deal in size, often have frequency requirement that must be met. This work discusses two missions that utilize this type of aperture technology, and then develops a Rayleigh-Ritz model that predicts the natural frequencies and mode shapes for a (nearly) flat and singly-curved reflector with unidirectional in-plane loading. The results are compared with NASTRAN analyses.

Introduction

NASA's mission challenges its scientists to understand and protect the Earth and to explore the universe. To fulfill NASA's mission, the country's scientists are increasingly demanding more and better information about the earth and the surrounding cosmos. As a result, technological solutions for these needs are increasingly requiring larger and larger apertures. The most demanding NASA customers for precision deployable structures technologies will be future large space systems for observation and remote sensing¹. These systems depend on an aperture which collects energy and concentrates it on a detector where the radiation and spectra can be measured. The size of the aperture determines the resolution to which an image can be made, the collecting area determines how faint an object can be detected, and the precision to which the aperture holds its figure determines how well the energy is directed onto the detectors. The planned missions cover the wavelength range from the visible to radio frequency, with increasing precision required for shorter wavelengths and increasing size required for longer wavelengths.

One proposed technological solution for constructing such apertures involves the use of tensioned cylindrical membranes. By applying tension in the "straight" direction, a singly-curved reflector can be constructed. Two recent studies of this geometry were the Dual Anamorphic Reflector Telescope (DART) and the Advanced Precipitation Radar Antenna (APRA).

Dual Anamorphic Reflector Telescope

DART consists of two parabolic cylindrical-trough reflectors oriented perpendicular with respect to each other to produce a point focus, as shown in Figure 1.

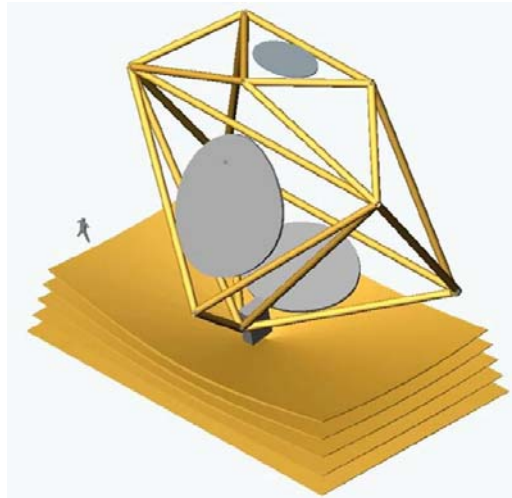


Figure 1: Concept of a 10m DART Architecture with Passive V-groove Cooling

Such a surface can be formed by bending the reflective surface along only one axis, and the system can be designed to produce a completely unobscured aperture. The focal lengths of the two individual reflectors are unequal for this system to focus (hence the need for anamorphic optics). The aberrations of the system are identical to those of an off-axis paraboloid; hence it is not surprising that coma is the dominant aberration.

The DART concept is being developed for a future Single Aperture Far-Infrared (SAFIR) space mission²⁻⁷. With a cryogenically cooled 10-meter class primary mirror and detectors providing high sensitivity in the 40-1000 μm wavelength range, SAFIR would enable scientists to probe the structure and evolution of the first stars and galaxies, to understand the interactions between black-holes and their host galaxies, and to observe the birth of stars and planetary systems. The principle challenge to making SAFIR is its large cryogenic primary mirror. Keeping its mirror at less than 5 Kelvin is essential for making background-limited measurements in the far infrared. Such a telescope should have a large, cooled, unobstructed aperture and be in space, which means it must also be low mass and deployable. A traditional telescope uses a reflective coating supported by a high-quality substrate, which is usually glass or metal. To reduce mass, DART abandons the glass substrate, leaving only the reflective coating as a thin membrane. The membrane is shaped and constrained, both of which are accomplished by clamping at the edge, or boundary, and then stretching.

Advanced Precipitation Radar Antenna

The second concept, the APRA⁸, consists of a single parabolic cylindrical-trough reflector oriented so its focus is fed by a phased array line feed. Again the surface can be formed by bending the reflective surface along only one axis. Control of the surface

aberrations can be provided by adjusting the tensioning elements or by in-plane (surface parallel) actuation. The APRA concept is being developed for a future space-borne mission to measure rainfall world-wide. Dual-frequency Ka/Ku-band radar is used to measure precipitation and improve our understanding of worldwide weather. Figure 2 shows the APRA concept.

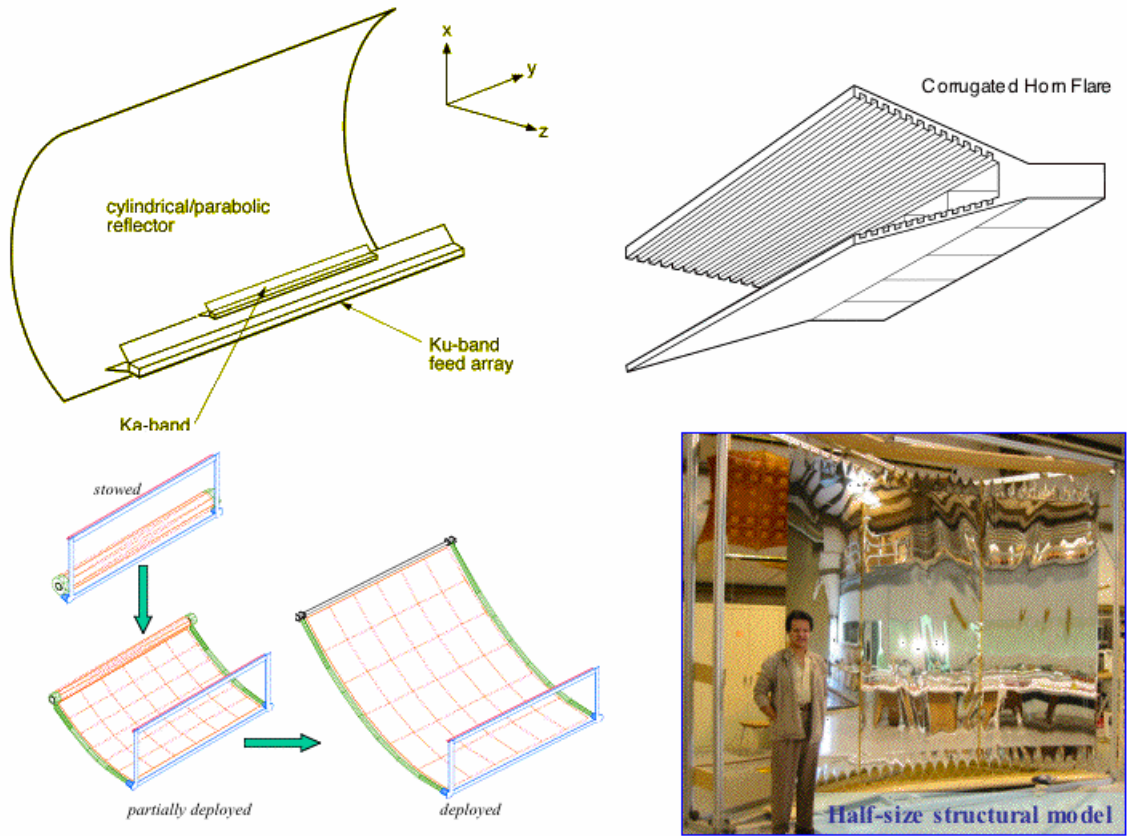


Figure 2: Advanced Precipitation Radar Antenna Concept and Model

In the bottom left, the unrolling deployment of the reflector is shown. For launch, the membrane is rolled onto a mandrel, and then once on-orbit, the reflector unrolls into the desired parabolic shape. A half-scale model, in the bottom right was built and tested to determine if the required surface precision was readily attainable.

Modeling of Reflector

To perform early mission designs using the DART, APRA or similar concepts, a simple, mathematical model is needed to determine the structural stiffness of the concept. Then trades can be made based upon stiffness requirements and other mission parameters. This paper represents a first step towards forming a simple mathematical estimation of the vibrational modes of a tensioned, singly-curved membrane. Efforts to predict the dynamic behavior of these types of structures typically involves modeling them as thin shells. These shells are taken to be shallow, singly-curved, isotropic, thin films that are

tensioned perpendicular to the direction of curvature through a clamped edge with the other two edges free from constraint. These boundary conditions are referred to as Clamped-Free-Clamped-Free (C-F-C-F). For a flat plate with such boundary conditions, there is a small amount of literature that summarizes the dynamic response⁹. However, the author is not aware of any that covers the transverse vibration of C-F-C-F shells in rectangular coordinates. Therefore, the focus of this work is to investigate the transverse vibrational behavior of an elastic thin, shallow shell subjected to in-plane traction. While the out of plane behavior is of primary concern, it is coupled to the in-plane response because of the curvature. Therefore an important component of this project is to understand both the in-plane¹⁰ and out-of-plane response¹¹⁻¹⁴. The appropriate energy functionals, strain energy, kinetic energy, and work done by external forces, are formulated from the 3D elasticity theory using classical shell theory, with Love's first approximation and ignoring transverse shear deformation. While the model was developed for a laminated composite material, simplifications are made to cover only isotropic behavior. After choosing a representative geometry and material, these expressions were calculated in *Mathematica*, and the eigenvalue problem solved numerically using the computer to determine the natural frequencies and mode shapes of both a flat and the curved reflector. These results are found to be in good agreement with NASTRAN analyses.

Shell Theory

In this work, the singly-curved reflector is modeled as a thin shallow shell, as depicted in Figure 3.

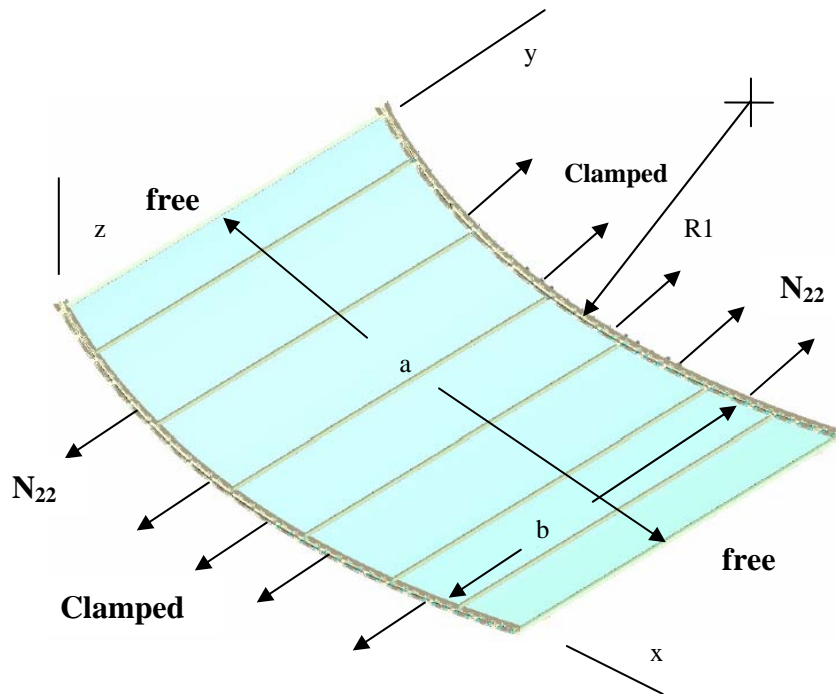


Figure 3: Singly-Curved Thin Shallow Shell

The boundary conditions along the curved edges ($y=0$ and $y=b$) are clamped, and along the flat edges ($x=0$ and $x=a$) are free (C-F-C-F). The Rayleigh-Ritz method is employed in this work to solve the free vibration problem of this shallow shell. This method involves determining the expression for the total energy (strain plus kinetic), Π , of the vibrating system, and then selecting appropriate admissible functions to represent the in-plane and out-of-plane deflections. These functions represent beam mode shapes in the C-C and F-F directions. Stationary values of the total potential energy are then found by minimizing with respect to the constants contained in the admissible functions such that

$$\frac{\partial \Pi}{\partial A_{mn}} = \frac{\partial \Pi}{\partial B_{mn}} = \frac{\partial \Pi}{\partial C_{mn}} = 0 \quad (1)$$

By grouping terms common to the constants A_{mn} , B_{mn} , and C_{mn} , one is left with the standard eigenvalue problem, with a mass and a stiffness matrix, which can be solved using standard methods to obtain the free vibration response of the shallow shell.

Energy Expressions

The derivation of the energy expressions for this problem begins with the strain energy for a 3D elastic shell continuum, expressed as

$$V = \frac{1}{2} \int \int \int_{x y z} (\sigma_{11}e_{11} + \sigma_{22}e_{22} + \sigma_{12}e_{12} + \sigma_{13}e_{13} + \sigma_{23}e_{23}) A_1 A_2 \left(1 + \frac{z}{R_1}\right) \left(1 + \frac{z}{R_2}\right) dx dy dz \quad (2)$$

A few simplifying assumptions can be made to reduce this 3D problem to a simpler yet accurate 2D representation for the specific shell under consideration in this work. First, the shell is singly-curved, thus R_2 equals infinity. Also, the shell is thin, so transverse shear is ignored (e_{13} and e_{23} equal zero). Next the shell is shallow, so $A_1=A_2=1$ and Love's 1st approximation is applicable, giving

$$\frac{z}{R_1} \approx \frac{z}{R_2} \approx 0 \quad (3)$$

and consequently the 3D strains can be represented by their 2D approximations

$$e_{11} = \varepsilon_{11} + zk_{11} \quad e_{22} = \varepsilon_{22} + zk_{22} \quad e_{12} = \gamma_{12} + zk_{12} \quad (4)$$

Here, ε_{ij} are midplane strains, and k_{ij} are changes in midplane curvatures. Next, if the shell is considered to be made of N total orthotropic layers for the purpose of generality, then the constitutive relations the k^{th} layer of this shell are

$$\begin{aligned}
\sigma_{11}^k &= \bar{Q}_{11}^k \varepsilon_{11} + \bar{Q}_{12}^k \varepsilon_{22} + \bar{Q}_{16}^k \gamma_{12} & \sigma_{22}^k &= \bar{Q}_{12}^k \varepsilon_{11} + \bar{Q}_{22}^k \varepsilon_{22} + \bar{Q}_{26}^k \gamma_{12} \\
\sigma_{12}^k &= \bar{Q}_{16}^k \varepsilon_{11} + \bar{Q}_{26}^k \varepsilon_{22} + \bar{Q}_{66}^k \gamma_{12}
\end{aligned} \tag{5}$$

These stresses and 2D strains are now substituted into the strain energy expression in Eq. 2 and integrated over the thickness of each layer and summed over the N total layers in order to reduce the problem completely from 3D to 2D. The resulting strain energy expression is

$$\begin{aligned}
V &= \frac{1}{2} \iint_{x \ y} \left(\sum_{k=1}^N \int_{h_{k-1}}^{h_k} [(\bar{Q}_{11}^k \varepsilon_{11} + \bar{Q}_{12}^k \varepsilon_{22} + \bar{Q}_{16}^k \gamma_{12}) \varepsilon_{11} + (\bar{Q}_{12}^k \varepsilon_{11} + \bar{Q}_{22}^k \varepsilon_{22} + \bar{Q}_{26}^k \gamma_{12}) \varepsilon_{22} \right. \\
&\quad \left. + (\bar{Q}_{16}^k \varepsilon_{11} + \bar{Q}_{26}^k \varepsilon_{22} + \bar{Q}_{66}^k \gamma_{12}) \gamma_{12} \right] dz \Big) dx dy
\end{aligned} \tag{6}$$

Next, if the linear strain-displacement relationships for a 2D shallow shell with the simplifications described above are

$$\begin{aligned}
\varepsilon_{11} &= \frac{\partial u}{\partial x} + \frac{w}{R_1} & \varepsilon_{22} &= \frac{\partial v}{\partial y} & \gamma_{12} &= \frac{\partial u}{\partial y} + \frac{\partial v}{\partial x} \\
k_{11} &= -\frac{\partial^2 w}{\partial x^2} & k_{22} &= -\frac{\partial^2 w}{\partial y^2} & k_{12} &= -2\frac{\partial^2 w}{\partial x \partial y}
\end{aligned} \tag{7}$$

and the following standard stiffness definitions for laminated structures are used,

$$A_{ij} = \sum_{k=1}^N \bar{Q}_{ij}^k (h_k - h_{k-1}) \quad B_{ij} = \frac{1}{2} \sum_{k=1}^N \bar{Q}_{ij}^k (h_k^2 - h_{k-1}^2) \quad D_{ij} = \frac{1}{3} \sum_{k=1}^N \bar{Q}_{ij}^k (h_k^3 - h_{k-1}^3) \tag{8}$$

then the strain energy of the shell becomes

$$\begin{aligned}
V &= \frac{1}{2} \iint_{x \ y} \left[A_{11} \left(\left(\frac{\partial u}{\partial x} \right)^2 + 2 \frac{\partial u}{\partial x} \frac{w}{R_1} + \frac{w^2}{R_1^2} \right) + 2A_{12} \left(\frac{\partial u}{\partial x} \frac{\partial v}{\partial y} + \frac{\partial v}{\partial y} \frac{w}{R_1} \right) + 2A_{16} \left(\frac{\partial u}{\partial x} \frac{\partial v}{\partial x} + \frac{\partial u}{\partial x} \frac{\partial u}{\partial y} + \frac{\partial u}{\partial y} \frac{w}{R_1} + \frac{\partial v}{\partial x} \frac{w}{R_1} \right) \right. \\
&\quad + A_{22} \left(\frac{\partial v}{\partial y} \right)^2 + 2A_{26} \left(\frac{\partial v}{\partial x} \frac{\partial v}{\partial y} + \frac{\partial v}{\partial y} \frac{\partial u}{\partial y} \right) + A_{66} \left(\left(\frac{\partial v}{\partial x} \right)^2 + 2 \frac{\partial v}{\partial x} \frac{\partial u}{\partial y} + \left(\frac{\partial u}{\partial y} \right)^2 \right) \Big] dx dy + \iint_{x \ y} \left[B_{11} \left(-\frac{\partial u}{\partial x} \frac{\partial^2 w}{\partial x^2} - \frac{w}{R_1} \frac{\partial^2 w}{\partial x^2} \right) \right. \\
&\quad + B_{12} \left(-\frac{\partial v}{\partial y} \frac{\partial^2 w}{\partial x^2} - \frac{\partial u}{\partial x} \frac{\partial^2 w}{\partial y^2} - \frac{w}{R_1} \frac{\partial^2 w}{\partial y^2} \right) + B_{16} \left(-2 \frac{\partial u}{\partial x} \frac{\partial^2 w}{\partial x \partial y} - 2 \frac{w}{R_1} \frac{\partial^2 w}{\partial x \partial y} - \frac{\partial v}{\partial x} \frac{\partial^2 w}{\partial x^2} - \frac{\partial u}{\partial y} \frac{\partial^2 w}{\partial x^2} \right) \\
&\quad + B_{22} \left(-\frac{\partial v}{\partial y} \frac{\partial^2 w}{\partial y^2} \right) + B_{26} \left(-2 \frac{\partial v}{\partial y} \frac{\partial^2 w}{\partial x \partial y} - \frac{\partial v}{\partial x} \frac{\partial^2 w}{\partial y^2} - \frac{\partial u}{\partial y} \frac{\partial^2 w}{\partial y^2} \right) + B_{66} \left(-2 \frac{\partial v}{\partial x} \frac{\partial^2 w}{\partial x \partial y} - 2 \frac{\partial u}{\partial y} \frac{\partial^2 w}{\partial x \partial y} \right) \Big] dx dy \\
&\quad + \frac{1}{2} \iint_{x \ y} \left[D_{11} \left(\frac{\partial^2 w}{\partial x^2} \right)^2 + 2D_{12} \left(\frac{\partial^2 w}{\partial x^2} \frac{\partial^2 w}{\partial y^2} \right) + 4D_{16} \left(\frac{\partial^2 w}{\partial x^2} \frac{\partial^2 w}{\partial x \partial y} \right) + D_{22} \left(\frac{\partial^2 w}{\partial y^2} \right)^2 + 4D_{26} \left(\frac{\partial^2 w}{\partial y^2} \frac{\partial^2 w}{\partial x \partial y} \right) + 4D_{66} \left(\frac{\partial^2 w}{\partial x \partial y} \right)^2 \right] dx dy
\end{aligned} \tag{9}$$

Equation 9 now represents the strain energy in terms of the orthotropic stiffnesses and displacements of a laminated composite thin shallow shell. However, the reflectors typically considered for the purpose of this research effort are thin metallic or polymer single layer films. Thus they have $N=1$ and behave in an isotropic manner. In such a case, there is no shear-extension coupling or bend-twist coupling, hence

$$A_{16} = A_{26} = D_{16} = D_{26} = 0 \quad (10)$$

Since the single isotropic layer is symmetric with respect to its midplane, there is no bending-extension coupling, or,

$$B_{ij} = 0 \quad (11)$$

The remaining non-zero in-plane extensional stiffnesses reduce to

$$A_{11} = A_{22} = \frac{Et}{1-\nu^2} \quad A_{12} = \frac{\nu Et}{1-\nu^2} \quad A_{66} = \frac{1-\nu}{2} \frac{Et}{1-\nu^2} \quad (12)$$

while the remaining bending stiffnesses become

$$D_{11} = D_{22} = \frac{Et^3}{12(1-\nu^2)} \quad D_{12} = \frac{\nu Et^3}{12(1-\nu^2)} \quad D_{66} = \frac{1-\nu}{2} \frac{Et^3}{12(1-\nu^2)} \quad (13)$$

With these isotropic simplifications, the strain energy becomes

$$\begin{aligned} V = & \frac{1}{2} \frac{Et}{(1-\nu^2)} \iint_{x,y} \left[\left(\frac{\partial u}{\partial x} \right)^2 + 2 \frac{\partial u}{\partial x} \frac{w}{R_1} + \left(\frac{w}{R_1} \right)^2 + 2\nu \left(\frac{\partial u}{\partial x} \frac{\partial v}{\partial y} + \frac{\partial v}{\partial y} \frac{w}{R_1} \right) + \left(\frac{\partial v}{\partial y} \right)^2 \right. \\ & \left. + \frac{1-\nu}{2} \left[\left(\frac{\partial v}{\partial x} \right)^2 + 2 \frac{\partial v}{\partial x} \frac{\partial u}{\partial y} + \left(\frac{\partial u}{\partial y} \right)^2 \right] \right] dydx + \frac{1}{2} \cdot \frac{Et^3}{12(1-\nu^2)} \iint_{x,y} \left[\left(\frac{\partial^2 w}{\partial x^2} \right)^2 \right. \\ & \left. + 2\nu \left(\frac{\partial^2 w}{\partial x^2} \frac{\partial^2 w}{\partial y^2} \right) + \left(\frac{\partial^2 w}{\partial y^2} \right)^2 + 2(1-\nu) \left(\frac{\partial^2 w}{\partial x \partial y} \right)^2 \right] dydx \end{aligned} \quad (14)$$

The strain energy from external in-plane tractions N_{11} , N_{22} , and N_{12} on the edges of the shell is

$$V_{ext} = \frac{1}{2} \iint_{x,y} \left[N_{11} \left(\frac{\partial w}{\partial x} \right)^2 + N_{22} \left(\frac{\partial w}{\partial y} \right)^2 + 2N_{12} \frac{\partial w}{\partial x} \frac{\partial w}{\partial y} \right] dydx \quad (15)$$

However, for the current problem, only N_{22} is nonzero. Neglecting in-plane inertia, the vibration energy comes from transverse motion only, such that

$$V_{vib} = \frac{-\omega^2 \rho t}{2} \iint_{x,y} w^2 dy dx \quad (16)$$

With Equations 14-16, the total potential energy of the vibrating system is then

$$\Pi = V + V_{ext} + V_{vib} \quad (17)$$

Rayleigh-Ritz Method

Equation 17 expresses the total potential energy for the vibrating shell in terms of the displacements u , v , and w . The Rayleigh-Ritz method represents these displacements as linear series of admissible functions and adjusts the coefficients in the series in order to minimize the total potential energy as given by Equation 1. The admissible functions must meet the artificial boundary conditions but not necessarily the natural boundary conditions. For the singly curved shallow shell under consideration in this paper, the in-plane displacements are approximated as

$$u(x, y) = \sum_{m=1}^M \sum_{n=1}^N A_{mn} X_m^u(x) Y_n^u(y) = \sum_{m=1}^M \sum_{n=1}^N A_{mn} \cos \frac{m\pi x}{a} \sin \frac{n\pi y}{b} \quad (18)$$

$$v(x, y) = \sum_{m=1}^M \sum_{n=1}^N B_{mn} X_m^v(x) Y_n^v(y) = \sum_{m=1}^M \sum_{n=1}^N B_{mn} \cos \frac{m\pi x}{a} \sin \frac{n\pi y}{b} \quad (19)$$

where X^u and X^v represent the axial vibration modes of a free-free beam in the x and y directions, respectively, and Y^u and Y^v represent clamped-clamped beam modes in the x and y directions, respectively. The out of plane deflection is approximated as

$$w(x, y) = \sum_{m=1}^M \sum_{n=1}^N C_{mn} X_m^w(x) Y_n^w(y) \quad (20)$$

where the functions X^w and Y^w are mode shapes for the transverse vibration of a free-free and a clamped-clamped beam, respectively, given by

$$\begin{aligned} X_1^w(x) &= 1 & X_2^w(x) &= \sqrt{3} \left(1 - \frac{2x}{a} \right) \\ X_m^w(x) &= \left[\cosh \frac{\lambda_m x}{a} + \cos \frac{\lambda_m x}{a} - \sigma_m \left(\sinh \frac{\lambda_m x}{a} + \sin \frac{\lambda_m x}{a} \right) \right] \quad (m = 3, 4, 5, \dots) \end{aligned} \quad (21)$$

and

$$Y_n^w(y) = \left[\cosh \frac{\mu_n y}{b} - \cos \frac{\mu_n y}{b} - \beta_n \left(\sinh \frac{\mu_n y}{b} - \sin \frac{\mu_n y}{b} \right) \right] \quad (n = 1, 2, 3, \dots) \quad (22)$$

The first two expressions in Equation 21 represent rigid body modes for the free-free beam. Careful examination of these approximation equations shows that they satisfy the required geometric boundary conditions.

Eigenvalue Problem

At this point, the approximate functions in Equations 18-20 are substituted into the total potential energy from Equation 17, requiring many partial derivatives. Taking the partial derivatives required to minimize the total potential energy per Equation 1 results in the matrix eigenvalue problem

$$\begin{bmatrix} K_{mnpq}^{uu} & K_{mnpq}^{uv} & K_{mnpq}^{uw} \\ \text{sym.} & K_{mnpq}^{vv} & K_{mnpq}^{vw} \\ \text{sym.} & \text{sym.} & K_{mnpq}^{ww} \end{bmatrix} \begin{bmatrix} A_{pq} \\ B_{pq} \\ C_{pq} \end{bmatrix} - \lambda^2 \begin{bmatrix} M_{mnpq}^{uu} & 0 & 0 \\ 0 & M_{mnpq}^{vv} & 0 \\ 0 & 0 & M_{mnpq}^{ww} \end{bmatrix} = 0 \quad (23)$$

where the stiffness matrix components are

$$\begin{aligned} K_{mnpq}^{uu} &= \frac{Et}{(1-\nu^2)} \int_0^b \int_0^a \left[X_m^{u'} Y_n^u X_p^{u'} Y_q^u + \frac{1-\nu}{2} X_m^u Y_n^{u'} X_p^u Y_q^{u'} \right] dx dy \\ K_{mnpq}^{uv} &= \frac{Et}{(1-\nu^2)} \int_0^b \int_0^a \left[\nu X_m^{u'} Y_n^u X_p^v Y_q^{v'} + \frac{1-\nu}{2} X_m^u Y_n^{u'} X_p^{v'} Y_q^v \right] dx dy \\ K_{mnpq}^{uw} &= \frac{Et}{R_1(1-\nu^2)} \int_0^b \int_0^a \left[X_m^{u'} Y_n^u X_p^w Y_q^w \right] dx dy \\ K_{mnpq}^{vv} &= \frac{Et}{(1-\nu^2)} \int_0^b \int_0^a \left[X_m^v Y_n^{v'} X_p^v Y_q^{v'} + \frac{1-\nu}{2} X_m^{v'} Y_n^v X_p^v Y_q^v \right] dx dy \\ K_{mnpq}^{vw} &= \frac{Et}{R_1(1-\nu^2)} \int_0^b \int_0^a \left[\nu X_m^v Y_n^{v'} X_p^w Y_q^w \right] dx dy \\ K_{mnpq}^{ww} &= \frac{Et}{R_1^2(1-\nu^2)} \int_0^b \int_0^a \left[X_m^w Y_n^w X_p^w Y_q^w \right] dx dy + \frac{Et^3}{12(1-\nu^2)} \int_0^b \int_0^a \left[X_m^{w''} Y_n^w X_p^{w''} Y_q^w + X_m^w Y_n^{w''} X_p^w Y_q^{w''} \right. \\ &\quad \left. + \nu \left(X_m^w Y_n^{w''} X_p^{w''} Y_q^w + X_m^{w''} Y_n^w X_p^w Y_q^{w''} \right) + 2(1-\nu) X_m^{w'} Y_n^{w'} X_p^{w'} Y_q^{w'} \right] dx dy + N_{22} \int_0^b \int_0^a \left[X_m^w Y_n^{w'} X_p^w Y_q^{w'} \right] dx dy \end{aligned} \quad (24)$$

and the only nonzero mass matrix component (neglecting in-plane inertia) is

$$M_{mnpq}^{ww} = \rho t \int_0^b \int_0^a [X_m^w Y_n^w X_p^w Y_q^w] dx dy \quad (25)$$

The mass and stiffness matrices can now be calculated in *Mathematica*, and the eigenvalue problem solved in the standard way in order to determine the natural frequencies and mode shapes of the curved reflector panel.

Numerical Results

In this section, a representative set of geometric and material properties are chosen for use with the model developed above. Such an approach allows for the solution to the eigenvalue problem, thus determining numerical results for the natural frequencies and mode shapes of the selected system. Since many curved reflectors are made from thin metallic films, the material properties of aluminum are considered for this numerical investigation. These properties, along with the selected geometry are presented in Table 1.

Table 1: Material and Geometric Properties

Property	Value
Modulus, E , GPa	70
Poisson Ratio, ν	0.33
Density, ρ , kg/m ³	2700
Length, a , m	0.7
Length, b , m	0.7
Radius of Curvature, R_1 , m	3
Thickness, t , m	6.35x10 ⁻⁵ to 6.35x10 ⁻²

First, a flat plate is considered, showing that the elasticity model is in agreement with finite element results, and then the more complicated behavior of a the curved panel is predicted.

Finite Element Analysis

The commercially-available finite element software NASTRAN was used to model the systems under consideration for this numerical investigation. The finite element models of the flat plates contained 900 CQUAD 4 plate structural elements, while the curved panel models consisted of 2450 structural elements of the same type. After defining the geometry and element meshing, all six degrees of freedom (three translational and 3 rotational) were restrained along the clamped edges $y=0$ and $y=b$. As the other edges are free, no degrees of freedom were restricted on those edges. Due to time constraints on the publication of this work, it was not possible to perform NASTRAN analyses with applied in-plane loads for either the flat plate or the curved panel. Such investigation will form the basis for a future work.

Flat Plate with Zero In-Plane Loads

The solution to a flat plate with C-F-C-F boundary conditions is found from the elasticity model developed above by setting the curvature, R_1 equal to zero. This simplification effectively decouples the in-plane and out-of-plane portions of the problem, and allowing for a much simpler solution. It is for this reason that tabulated results for this type of system are available in Blevins⁹. The results of these three methods are presented in Table 2.

Table 2: Natural Frequencies of C-F-C-F Plates of Various Thicknesses

Natural Frequency, Hz									
Mode Number	Method								
	Blevins			Rayleigh-Ritz			FEA		
	Thickness, m								
	6.35E-05	6.35E-04	6.35E-03	6.35E-05	6.35E-04	6.35E-03	6.35E-05	6.35E-04	6.35E-03
1	0.7152	7.152	71.52	0.7185	7.185	71.85	0.7103	7.103	70.973
2	0.852	8.52	85.2	0.8422	8.422	84.22	0.84	8.398	83.856
3	1.402	14.02	140.22	1.3967	13.967	139.67	1.382	13.819	137.883
4	1.974	19.74	197.41	1.9806	19.806	198.06	1.961	19.607	195.764
5	2.169	21.69	216.94	2.1489	21.489	214.89	2.142	21.415	213.684

The three methods are in close agreement, and the frequency scales linearly with the thickness of the plate, as suggested by Blevin's formulation. Furthermore, the mode shapes are of the same shape regardless of the thickness, and are depicted in Figure 4 for the thinnest plate.

Flat Plate with Nonzero In-Plane Loads

The effect of applied in-plane loading was investigated for the flat plate using the approximation in Blevins⁹. The natural frequency for a plate with in-plane loads N_{11} and N_{22} is

$$f_{ij(\text{loads})}^{(\text{in-plane})} = \sqrt{f_{ij(\text{loads})}^{2(\text{No in-plane})} + \frac{N_{11}J_1}{4\rho t a^2} + \frac{N_{22}J_2}{4\rho t b^2}} \quad (26)$$

For this work, $N_{11}=0$, and J_2 is given by

$$J_2 = \begin{cases} 1.248 & (n=1) \\ \left(n + \frac{1}{2}\right)^2 \left(1 - \frac{2}{\pi \left(n + \frac{1}{2}\right)}\right) & (n > 1) \end{cases} \quad (27)$$

where n is the mode number corresponding to the j subscript on f_{ij} . For a square plate ($a=b$), $n=1, 2, 3, 1, 2, 4$. Using Blevin's formula for the unloaded natural frequency, Figure 5 presents the impact of in-plane tractions on the plate with $t=6.35 \times 10^{-4} \text{m}$.

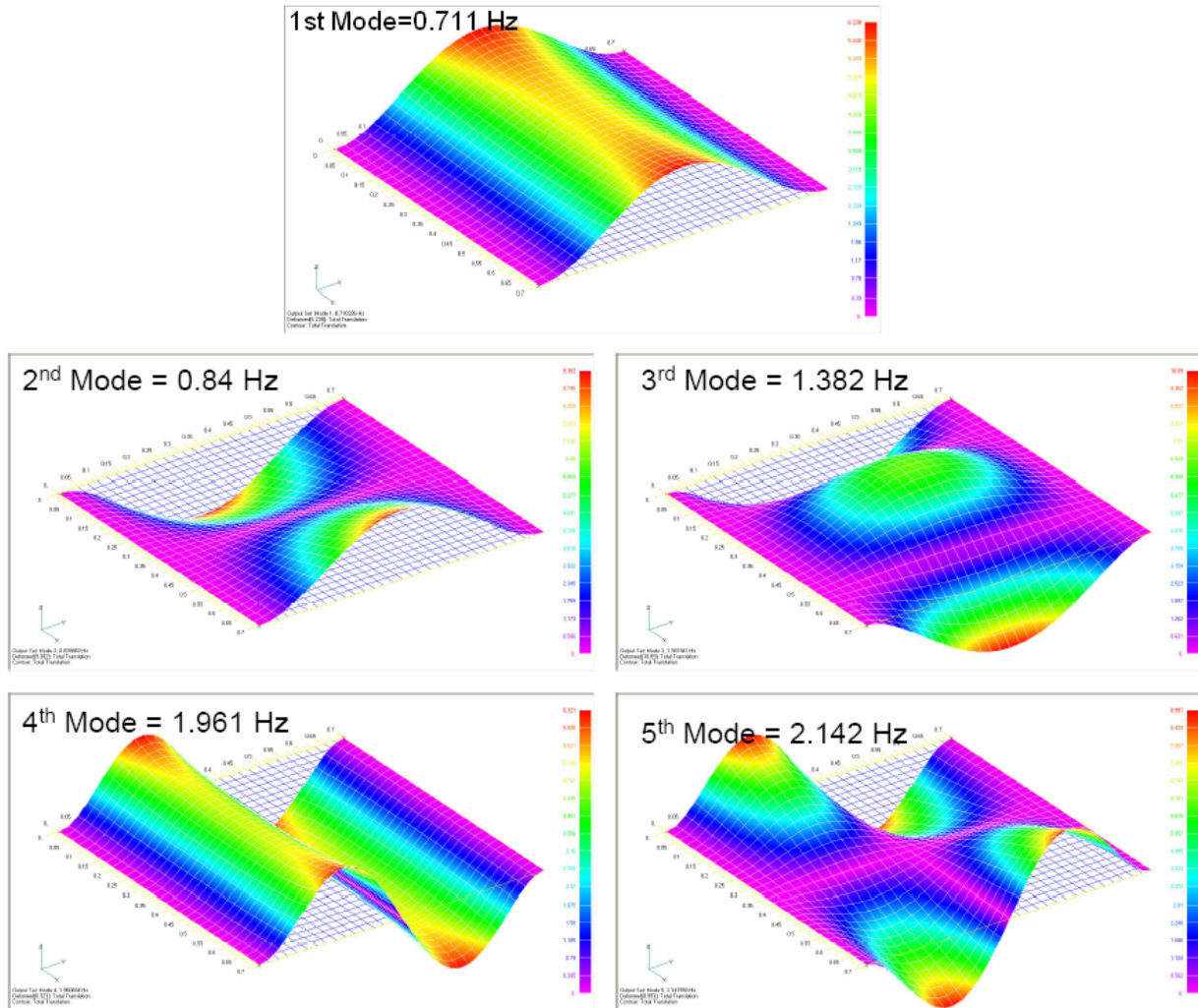


Figure 4: Mode Shapes from NASTRAN for Flat Plate

The range of traction loads ranges from zero up to around the Euler buckling load (if the load were to be compressive). Over this range fairly wide range, the changes in the natural frequencies of the flat plate vary widely from about 7% all the way up to nearly 100%. Thus, the amount of tensile in-plane load can have a significant impact on the dynamic response of the reflector system. The amount of effect depends on the particular mode, but it is clear that the in-plane load effects must be considered in any design analysis and need further investigation.

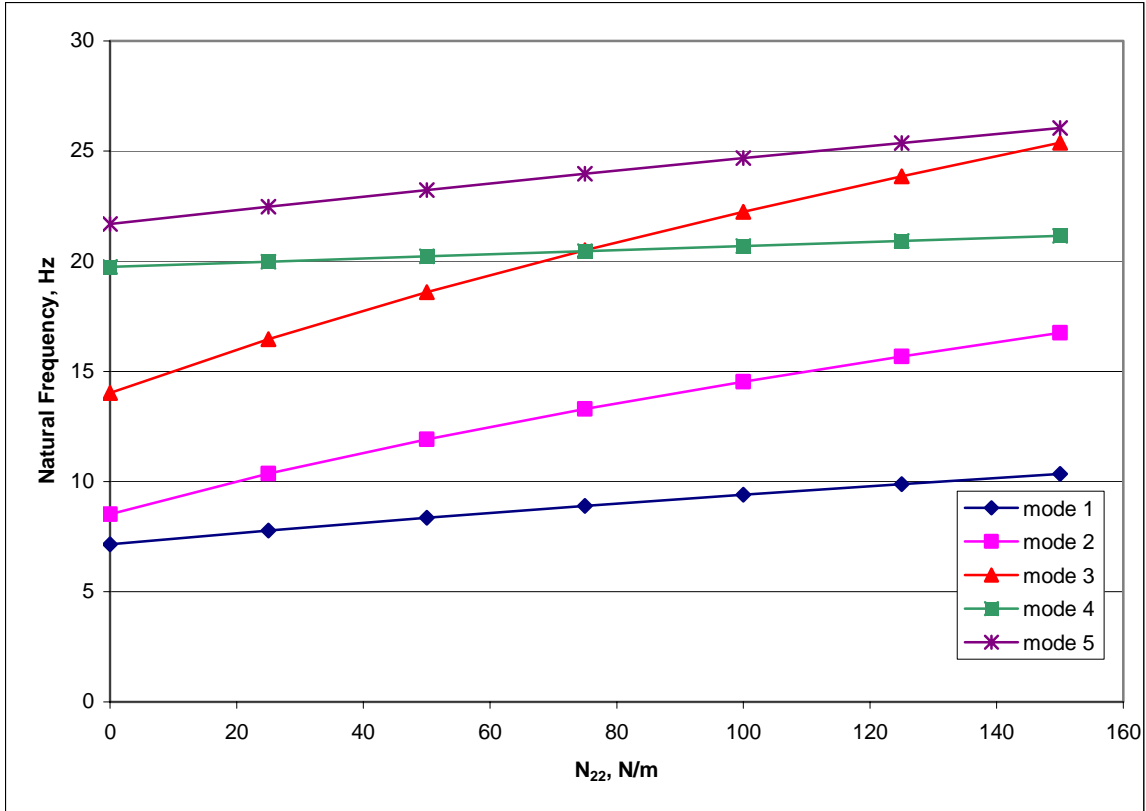


Figure 5: Effect of Unidirectional Traction on Natural Frequency of Flat Plate

Curved Panel with no In-Plane Loads

With confidence in the accuracy of the portion of the elasticity model that calculates the decoupled out-of-plane response for a flat plate, a nonzero value for the radius of curvature is now selected, as given in Table 1. As there are no readily available simplified, closed-form solutions for a curved panel with C-F-C-F boundary conditions, only the results from the Rayleigh-Ritz solution and finite element analysis are presented in Table 3.

Table 3: Natural Frequencies of C-F-C-F Singly-Curved Panels of Various Thicknesses

Mode Number	Natural Frequency, Hz							
	Method							
	Elasticity Model				FEA			
	Thickness, m							
	6.35E-05	6.35E-04	6.35E-03	6.35E-02	6.35E-05	6.35E-04	6.35E-03	6.35E-02
1					6.633	22.718	94.766	675.8732
2	Results not available at press time.				6.64	22.89	109.288	784.065
3	Results not available at press time.				11.423	43.824	168.953	1291.878
4	Results not available at press time.				11.451	44.195	232.036	1744.428
5	Results not available at press time.				16.5194	55.182	239.686	1889.496

From the natural frequencies predicted by the finite element analyses, the response of the curved panel does not scale linearly with the thickness. This behavior is seen from Figure 6, which presents the first mode shapes for the four thicknesses considered in this work.

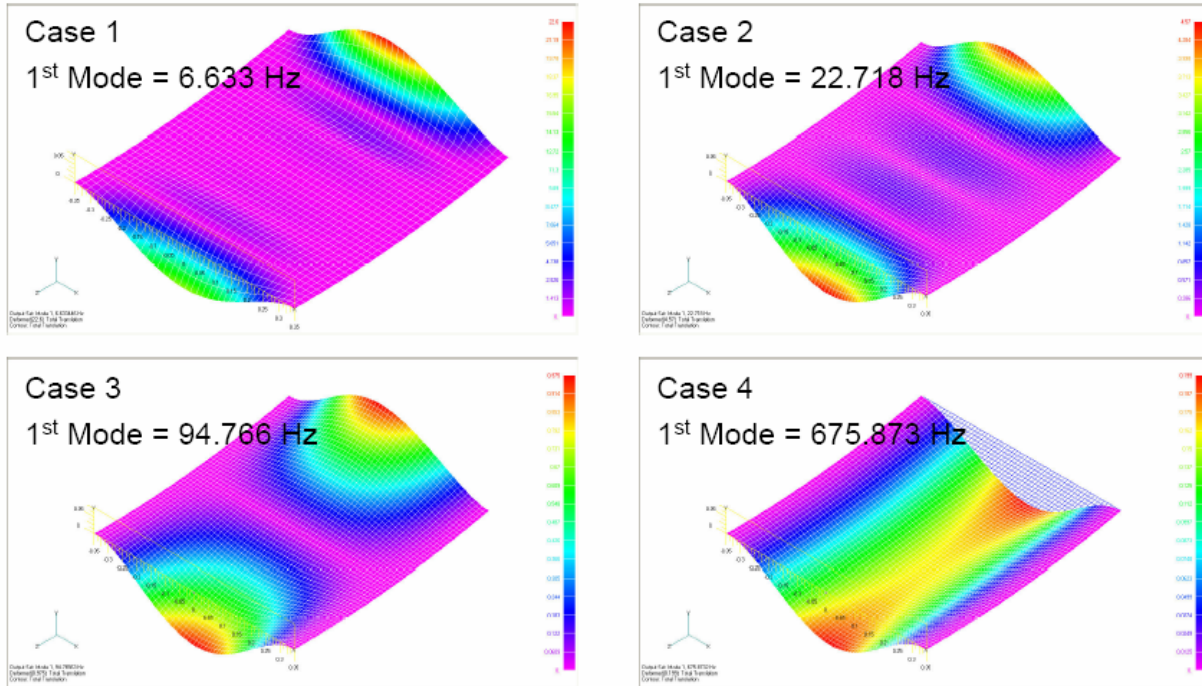


Figure 6: Fundamental Modes for Various Thickness Shallow Shells

For the thinner shells, the lowest mode shapes exhibit similar behavior. Specifically, the first beam mode is evident in the C-C direction, while the second beam mode (rigid body rotation) is evident in the F-F direction. However, the thickest shell has a different combination of beam mode shapes, namely the first mode in the C-C direction as well as the first mode (rigid body translation) in the F-F direction. This change in behavior could result from the thick (6.35 cm) plate, which is unlikely to follow the assumptions for thin shells as its length to thickness ratio is about 11. Indeed, the coupled in-plane-out-of-plane behavior is influenced by the thickness of the panel and changes the order in which the beam modes in each direction occur. In particular, the thinner panels seem to have a more complex response with higher beam modes occurring sooner, and some degenerate modes are evident even for the first five modes considered in this analysis. In Figures 6 and 7, the first two modes are combinations of the first beam mode in the C-C direction and the rigid body rotation and translation modes in the F-F direction, respectively. The third and fourth modes predicted by NASTRAN in Figure 7 are degenerate, in that they occur at essentially the same frequency. The linear combination of these two modes represents a match with the Rayleigh-Ritz solution, with second beam mode behavior in the C-C direction and rigid body rotation in the F-F direction. The lack of displacement for the fifth mode predicted by NASTRAN along one free

edge indicates another degenerate mode, but higher mode information is not available at this time. However, the third beam mode in the C-C direction is still evident. Clearly for this thinnest shell, the behavior is more complex and requires special precautions in the modeling, such as requiring more terms to the Rayleigh-Ritz series expansions, to ensure the correct behavior is predicted. However, more terms in the expansions creates large matrices that can become too computationally intensive to be handled numerically by the computer. For the thickness considered in Case 2 (Figure 8), the third and fourth modes exhibit second beam modes in the C-C direction and rigid body rotation and translation in the F-F direction, while the fifth mode has first beam mode behavior in the C-C direction and a much higher beam mode in the F-F direction. Additionally, the more complex behavior that includes very little displacement in the interior of the thinnest shells is likely due to the very low bending stiffness. While the free edges can move without restraint, the low bending stiffness does not allow this motion to propagate very far into the shell interior.

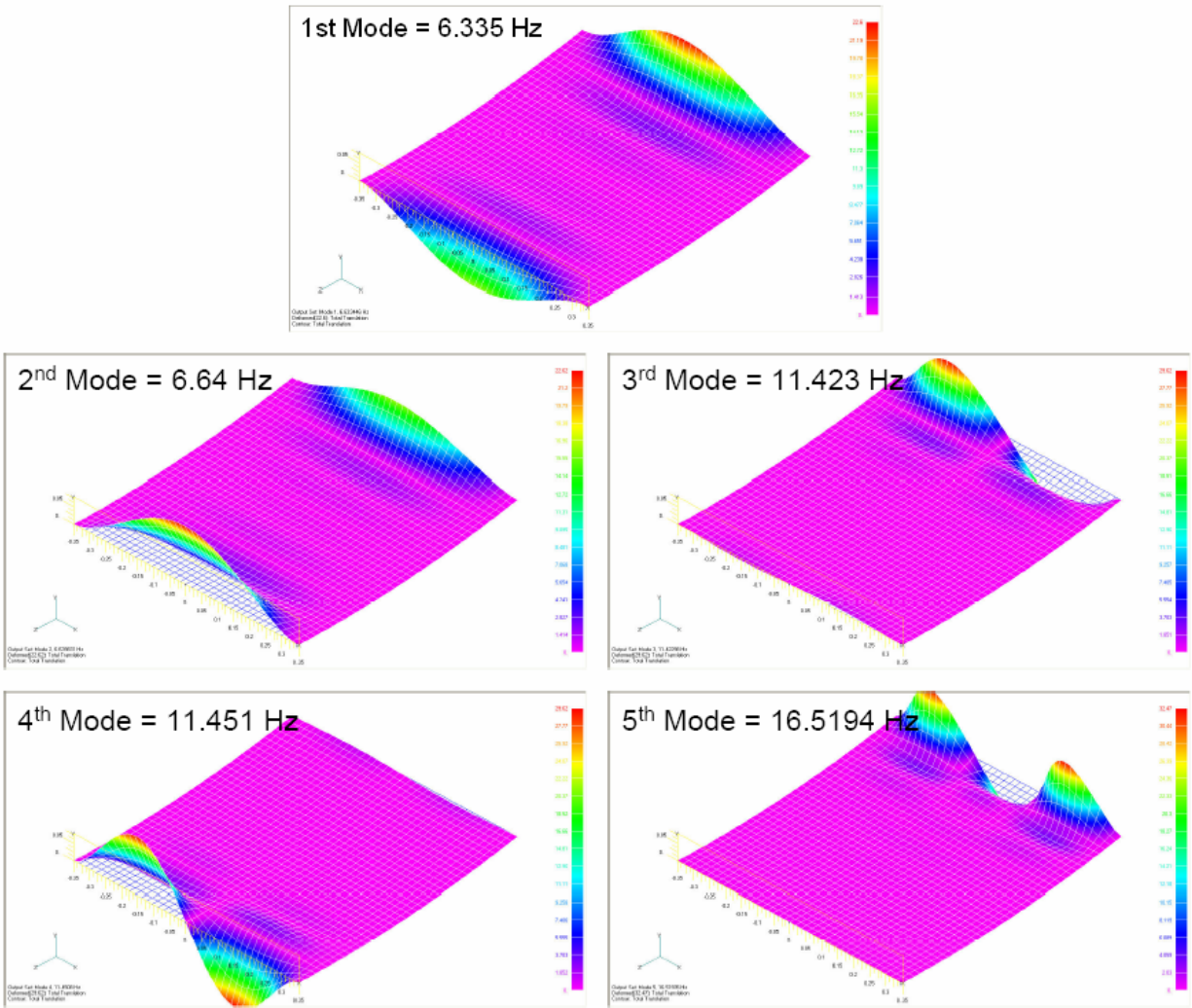


Figure 7: Five Lowest Mode Shapes for Curved Panel, Case 1, $t=6.35 \times 10^{-5}$ m

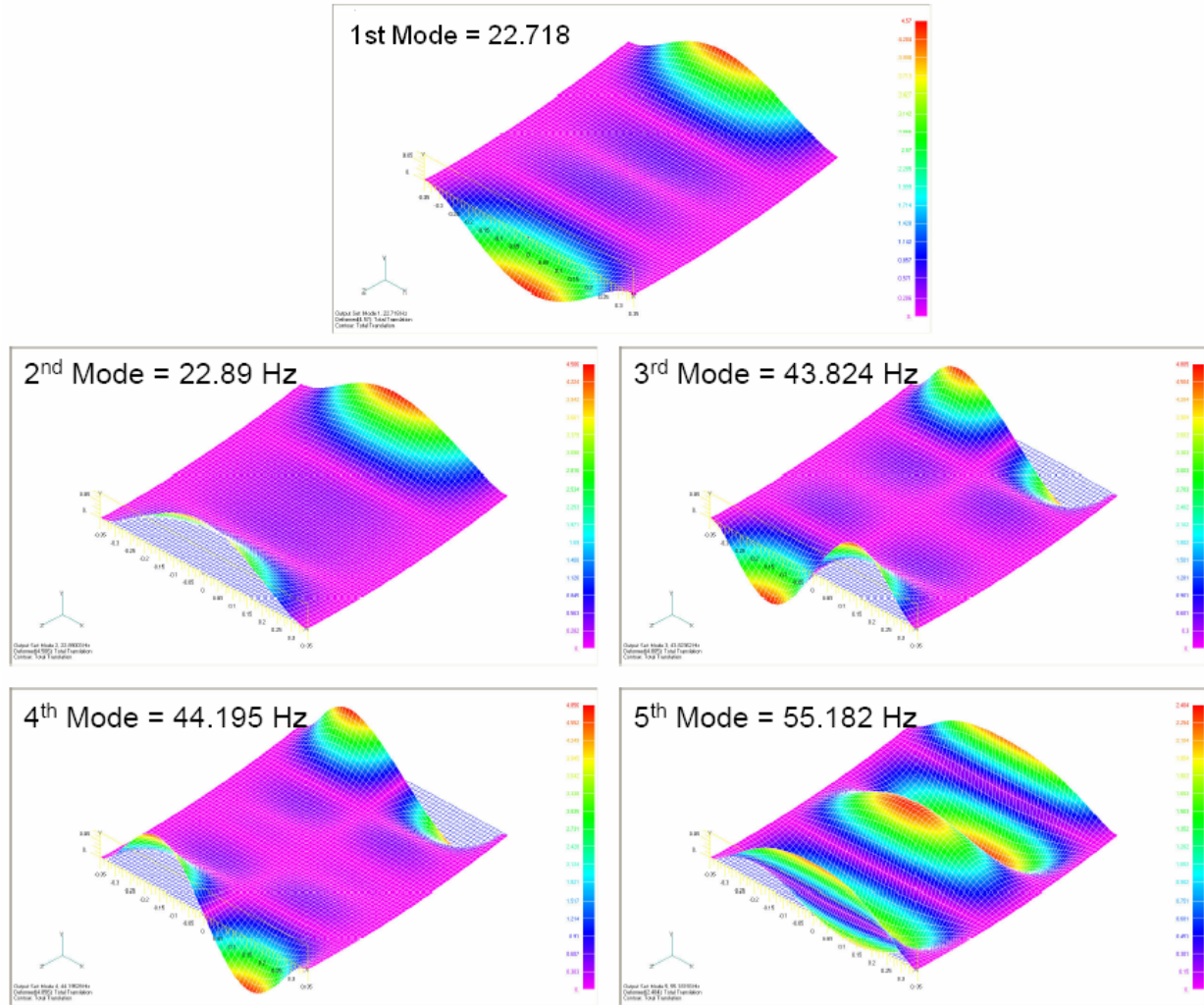


Figure 8: Five Lowest Mode Shapes for Curved Panel, Case 2, $t=6.35 \times 10^{-4}$ m

As noted earlier, the two thickest shells, whose mode shapes are shown in Figures 9 and 10, exhibit behavior, particularly in the shell interior that is more expected in terms of combinations of the lowest beam modes that compose the analytical response. Furthermore, each mode is distinct. For Case 3, the third mode shows first beam mode in the C-C direction and third beam mode (first non-rigid body mode) in the F-F direction, while the fourth and fifth modes exhibit second beam mode in the C-C direction and first rigid body rotation and translation in the F-F direction, respectively. Case 4, having the largest thickness, is a bit different than the other three cases. The rigid body rotation and translation are reversed with respect to Case 3 for modes 1 and 2. The third mode has the same characteristic shape, while the rigid body rotation and translation in the F-F direction for modes 4 and 5 are again reversed with respect to Case 3. The more complex behavior of the thinner shells requires more terms in the approximation functions for the Rayleigh Ritz method. Initial results indicate as many as 20×20 terms for u , v and w could be required to sufficiently capture the behavior.

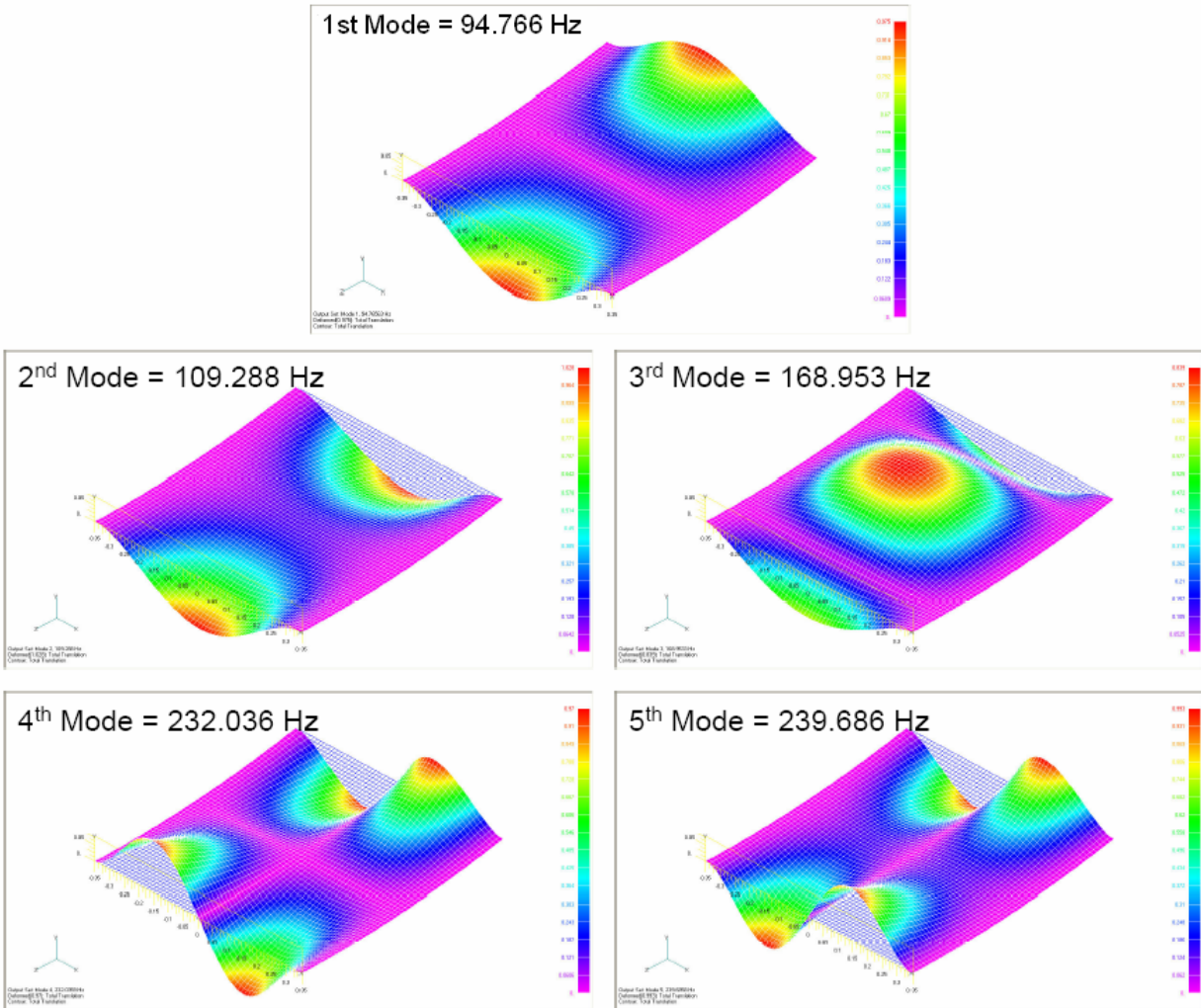


Figure 9: Five Lowest Mode Shapes for Curved Panel, Case 3, $t=6.35 \times 10^{-3}$ m

Conclusions

This work has presented two important NASA missions that utilize thin singly-curved membrane reflectors for telescope or radar applications. Preliminary sizing design for these structures is performed by using results from using the Rayleigh-Ritz method with an elasticity shell model presented in this work. It was found that the use of beam mode shapes in the two orthogonal directions is a suitable way to represent the shell approximation functions in the Rayleigh-Ritz method. While the behavior of the flat plate was easier to predict, the addition of a curvature in one direction made the analysis more difficult. The finite element analysis required additional elements, while the analytical model requires many more terms in the approximation functions. The natural frequencies of the flat plate scaled linearly with the thickness; however, the same was not true for the curved panel. The FEA results also indicate the presence or degenerate modes for the thinnest (membrane-like) curved panel, which indicates that the model is very sensitive to numerical variations. In contrast to the flat plate, much care must be taken to adequately capture the dynamics of the thin, curved reflector.

Acknowledgements

The research described in this publication was carried out at the Jet Propulsion Laboratory, California Institute of Technology, under a contract with the National Aeronautics and Space Administration.

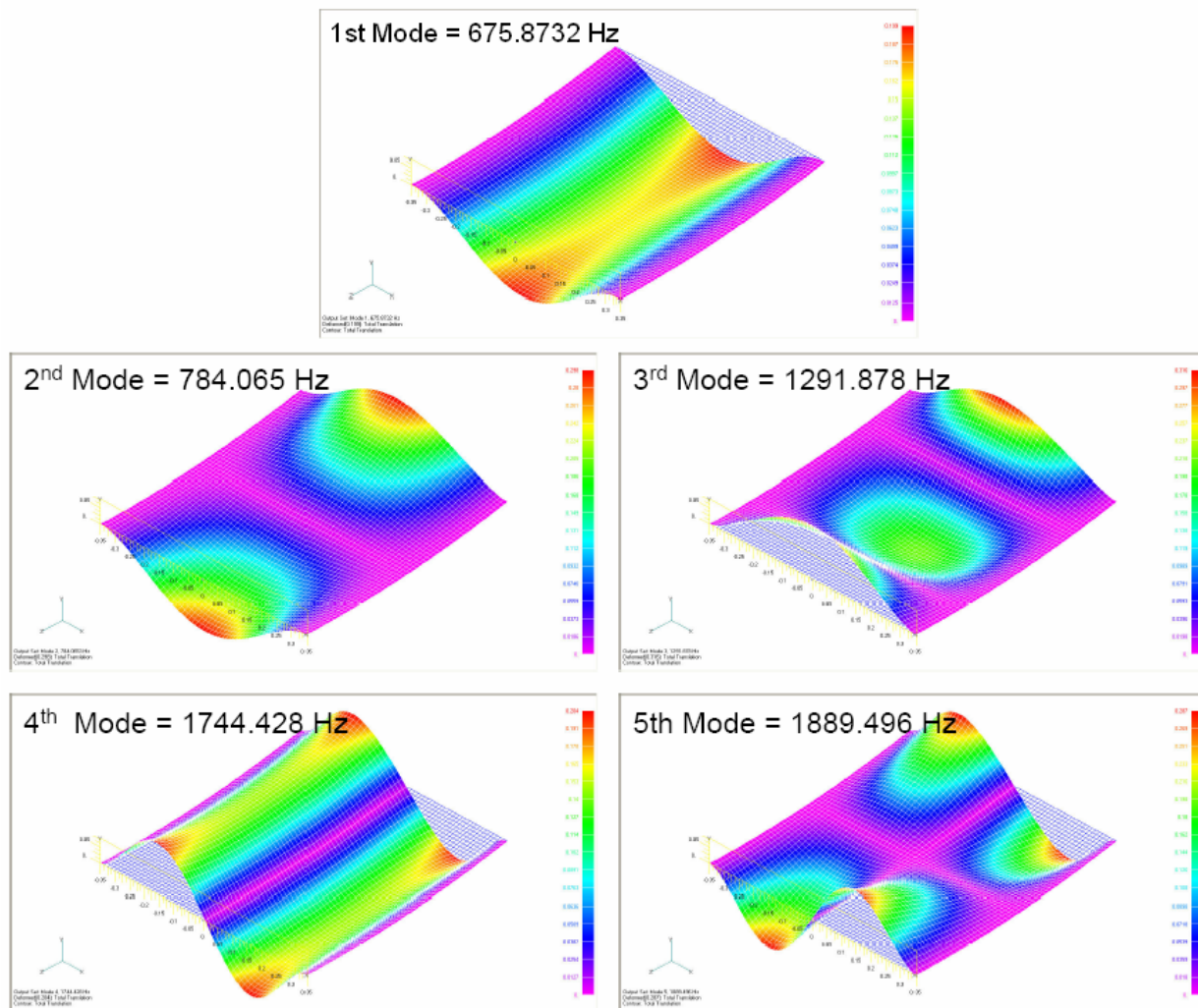


Figure 10: Five Lowest Mode Shapes for Curved Panel, Case 4, $t=6.35 \times 10^{-2}$ m

References

1. Agnes, G., and Dooley, J., "Precision Deployable Structures Technology for NASA Large Aperture Missions," AIAA-2004-5899, *Space 2004 Conference and Exhibit*, San Diego, CA, 28-30 September 2004, pp 1-7.
2. Dragovan, M., "The DART System for Far-IR/Submillimeter Space Missions," JPL White Paper, 2000.
3. Dragovan, M., 1999 Patent Application # USSN 6,502,944.
4. Dragovan, M., "Low Mass Density Far-IR Telescope Systems for Astrophysics," submitted to *Ap. J. Lett*, posted to *AstroPh #0001241*, 1999.

5. Sasian, J., "How to Approach the Design of a Bilateral Symmetric Optical System," *Optical Engineering*, Vol. 33, No. 6, pp. 2045-2051, June 1994.
6. Tolomeo, J., Cross, E. Jr., Sable, W., Decker, T., Putnam, D., Jamieson, T., Dragovan, M., Chmielewski, A., and Dooley, J., "Design and Test of Prototype DART System," *Proceedings of SPIE*, Vol. 4989, 2002.
7. Tolomeo, J., Loane, J., Tenerelli, D., Cross, G., Sable, B., Decker, T., Chan, K., Nelson, T., Joesph, W., Windes, C., Kokawa, D., Kamis, A., Dragovan, M., and Dooley, J., "Design and Test of a 2m x 4m DART System in RF," *Proceedings of SPIE*, Vol. 5166, 2003.
8. Lin, J., Sapna, G., III, Scarborough, S., and Lopez, B., "Advanced Precipitation Radar Antenna Singly Curved Parabolic Antenna Reflector Development," *Proceedings of the 44th AIAA/ASME/ASCE/AHS Structures, Structural Dynamics, and Materials Conference*, 7-10 April 2003, Norfolk, VA, AIAA-2003-1651.
9. Blevins, R., *Formulas for Natural Frequency and Mode Shape*, Krieger Publishing Company, Malabar, FL, 1979.
10. Farag, N., H., and Pan, J., 1999, "Modal Characteristics of In-Plane Vibration of Rectangular Plates," *Journal of the Acoustical society of America*, Vol. 105, No. 6, pp. 3295-3310.
11. Liew, K. M., and Lim, C. W., 1995, "A Ritz Vibration Analysis of Doubly-Curved Rectangular Shallow Shells Using a Refined First-Order Theory," *Computer Methods in Applied Mechanics and Engineering*, Vol. 127, pp. 145-162.
12. Abe, A., Kobayashi, Y., and Yamada, G., 2000, "Non-linear Vibration Characteristics of Clamped Laminated Shallow Shells," *Journal of Sound and Vibration*, Vol 234, No. 3, pp. 405-426.
13. Chun, L., and Lam, K. Y., 1995, "Dynamic Analysis of Clamped Laminated Curved Panels," *Composite Structures*, Vol. 30, pp. 389-398.
14. Leissa, A. W., and Qatu, M. S., 1991, "Equations of Elastic Deformation of Laminated Composite Shallow Shells," *Journal of Applied Mechanics*, Vol. 58, pp. 181-188.